

Current-Mode, WCDMA Channel Filter With In-Band Noise Shaping

Alberto Pirola, *Student Member, IEEE*, Antonio Liscidini, *Member, IEEE*, and Rinaldo Castello, *Fellow, IEEE*

Abstract—A novel class of filters (called pipe filters) that features in-band noise reduction is presented and a current mode bi-quad cell based on cross-connected cascoded devices is introduced. The presented solution gives in-band high-pass noise shaping and passive pre-filtering of out-of-band blockers. This results in both low in-band noise and high out-of-band IIP3. A 4th-order low-pass prototype in 90 nm CMOS for WCDMA application features 32 μV in-band noise (when integrated over the 2 MHz bandwidth as defined by the standard) and +36 dBm out-of-band IIP3 which results in a 75 dB SFDR with 1.25 mW power consumption. Active die area is 0.5 mm².

Index Terms—Continuous time filters, current filter, gm-C, high linearity, low noise, noise shaping, pipe filters, WCDMA.

I. INTRODUCTION

THE main goal of a wireless receiver is the detection of a low power signal among strong interferers present across the spectrum. Such an operation requires filtering out-of-band unwanted signals without deteriorating the desired signal present in the band of interest. This results in a very challenging spurious-free dynamic range (SFDR) requirement for the channel-select filter that has to manage at the same time a small signal and high level blockers. The core of a filter design is to take advantage of the noise–power–area and linearity trade-off to achieve the best match between the filter performance and the system requirements [1].

The amount of noise introduced by standard filters is proportional to kT/C and is concentrated in the filter passband, for this reason, once the noise filter floor is set, the amount of capacitance is roughly defined and, with it, a minimum in terms of area and power consumption [2]. The presence of a lower bound in the achievable in-band noise forces to have a minimum amount of gain (to be achieved with a sufficient linearity) before the filtering. This results in an increment of the power consumption not only for the filter, but also for the preceding stage, that performs the linear amplification. The solution presented in this paper aims to break these trade-offs by inserting an in-band zero in the transfer function for the input noise sources. This shapes the noise spectrum allowing to reduce the filter noise floor without increasing power consumption

and capacitance [3]. The concept of noise shaping was introduced for the first time by Tekin *et al.* [4] where a frequency-dependent negative resistance (FDNR) based active RC low-pass filter implementing such a behavior was presented. However at that time no experimental verification to prove its practical viability was provided. The first integrated prototype implementing a noise shaping filter that includes also a complete set of experimental measurements on both its noise and linearity was reported in [3] and it is the base for the present paper that further expands that original contribution. This last design realizes a gyrator-based low-pass filter implemented using gm-C techniques. Subsequently, a prototype implementing the FDNR-based design was also reported by the same authors [5]. In addition to in-band noise shaping, both the above structures filter a large amount of the out-of-band interferers before they enter the active devices, with a benefit on the SFDR.

The paper is structured as follows. In Section II, the concept of pipe filter is introduced and a first-order pipe filter topology is analyzed in terms of noise and linearity. A current bi-quad cell, based on the pipe filter concept, is proposed in Section III and analyzed in Section IV in further details. The design of the 4th-order WCDMA filter prototype is discussed in Section V and a complete set of experimental measurements is finally reported in Section VI.

II. PIPE FILTER

The current driven gm-C circuit shown in Fig. 1 implements a first-order low-pass filter (with a single real pole located at $\omega_p = g_m/C$, assuming $g_m \gg 1/R_S$). The key feature of this filter is the fact of producing a high-pass shaped output current noise spectrum $|I_{n,\text{out}}|^2$ due to the presence of an in-band zero in the transfer function from the transistor noise source to the output (Fig. 1). This behavior can be explained considering that, at very low frequencies, capacitance C is a high impedance, which forces the noise to re-circulate inside the transistor. On the contrary, at high frequencies, when the capacitance becomes a low impedance, all the current noise can flow to the output. More generally, the impedance associated with input current source creates an in-band degeneration for the transistor that minimizes noise and increases linearity, as it will be seen later.

An interesting way to describe this low-pass current filter is to consider it as a “pipeline” in which current is flowing and where a signal attenuation (frequency dependent) corresponds to a current loss through a leakage. Under this model, in the passband, the filter works as a lossless pipe where the input current is equal to the output one and thus no noise or distortion can be added to it [Fig. 2(a)]. On the contrary, in the stop band, the current leakage allows both noise and distortion component

Manuscript received March 11, 2010; revised June 17, 2010; accepted June 21, 2010. Date of current version August 25, 2010. This paper was approved by Associate Editor Andreas Kaiser. This work was supported by the Italian National Program FIRB under Contract RBAP06L4S5.

The authors are with the Dipartimento di Elettronica, Università degli Studi di Pavia, 27100 Pavia, Italy (e-mail: alberto.pirola@unipv.it; antonio.liscidini@unipv.it; rinaldo.castello@unipv.it).

Digital Object Identifier 10.1109/JSSC.2010.2056831

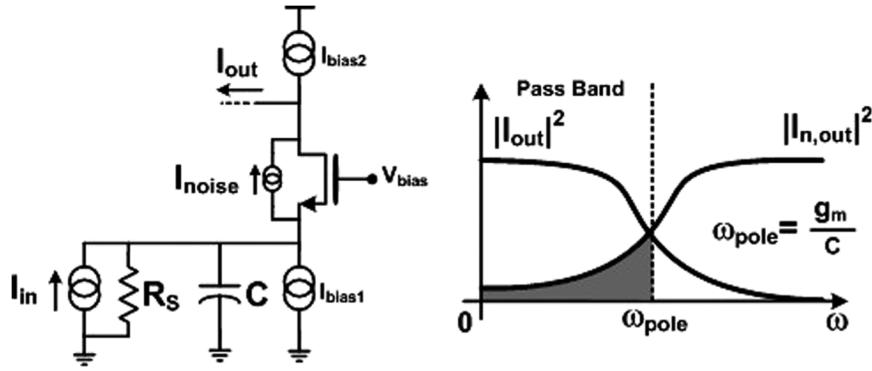


Fig. 1. First-order LP pipe filter.

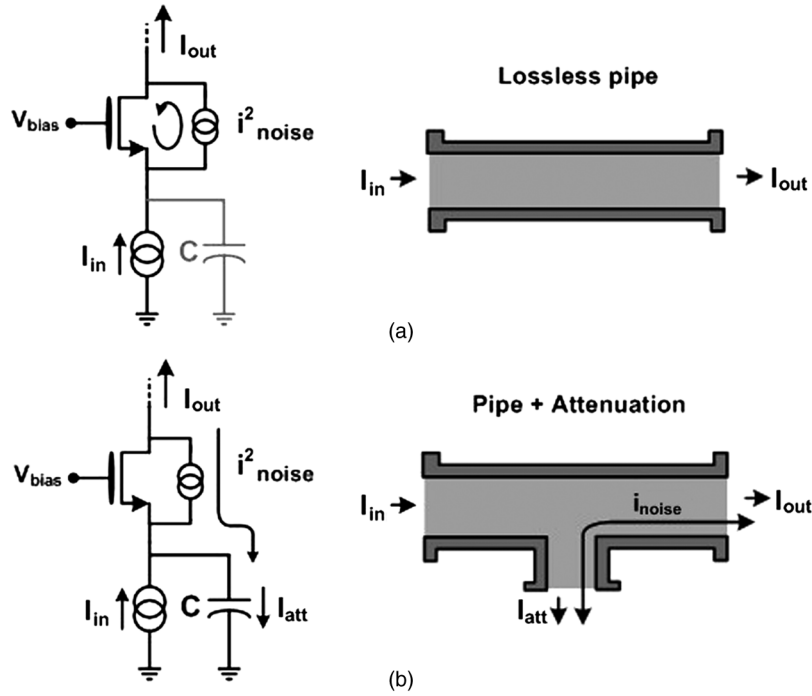


Fig. 2. Pipe filters: noise behavior.

to enter the pipe and reach the output. This occurs for example for the noise produced by the transistor when the capacitor is no more an open circuit [Fig. 2(b)]. In general, any kind of operation performed on the current that flows in the pipe can perturb the signal and introduce noise. An example is signal amplification that is obtained by injecting in the pipe an extra current proportional to the input current. For this reason, to ensure (at least ideally) that no noise is introduced in the passband, such kind of filter must have a unitary input to output transfer function. In practice this condition can never be perfectly satisfied due to the finite impedance associated with the signal source and with the bias circuitry (e.g., R_S , I_{bias1} and I_{bias2} in Fig. 1).

A. High-Pass Noise Shaping

The noise spectral density produced by the transistor at the filter output is equal to

$$\text{Noise}_{\text{out}}(\omega) \cong 4kT\gamma g_m \left| \frac{j\omega/\omega_p + 1/(g_m R_S)}{1 + j\omega/\omega_p} \right|^2 \quad (1)$$

where γ is the gamma coefficient of the FET thermal noise model. As expected, this expression displays a high-pass shape.

However, due to the finite driving impedance R_S , the zero in the noise transfer function is no located at DC but it is moved at $\omega_p/(g_m R_S)$.

The effect of the finite driver impedance is the introduction of an additional in-band loss that lets some extra noise to come out also in the passband. To better understand the impact of the zero on the total filter output noise, (1) can be rewritten as

$$\text{Noise}_{\text{out}}(\omega) \cong 4kT\gamma g_m \cdot \frac{(\omega/\omega_p)^2}{1 + (\omega/\omega_p)^2} + \frac{4kT\gamma}{g_m R_S^2} \cdot \frac{1}{1 + (\omega/\omega_p)^2} \quad (2)$$

where the total output noise is given by the sum of two terms: one still proportional to g_m and high-pass shaped, plus one inversely proportional to g_m which does not take any advantages from the zero introduced. The presence of a term inversely proportional to g_m sets a lower bound on the transconductance that can be used to synthesized the filter for a given total integrated output noise. In particular, integrating (2) in the filter passband (i.e., from 0 to ω_p) the second term exceeds the first one for $g_m < 2/R_S$.

In Appendix I it is shown that for the ideal case in which the zero is located at DC, this approach increases the in-band signal-to-noise ratio (SNR) by at least 5.6 dB compared to a classic first-order LP filter without noise shaping.

B. Intermodulation Distortion Mechanisms

Due to the same reason that produces an in-band noise shaping, no intermodulation product (IM) can be generated in the filter passband as long as the output current is equal to the input one (lossless-pipe). Notice that this is valid independently of the location of the interferers with respect to the filter passband. This mechanism can be verified evaluating the in-band third order intermodulation product (IM3) generated at ω_{IM3} (with ω_{IM3} located in the passband) by two tones located out of the filter passband at ω_1 and at $2\omega_1 - \omega_{IM3}$. Using Volterra's series approach ([6], [7]) and assuming for the transistor characteristic a Taylor expansion with g_i as the i th order coefficients, the power of the intermodulation term $|IM3(\omega_{IM3})|^2$ is given by

$$|I_{IM3}(\omega_{IM3})|^2 \approx \left| \frac{j\omega_{IM3}}{\omega_p} + \frac{1}{g_m R_S} \right|^2 |X(\omega_1, \omega_p)|^2 I_1^2 I_2 \quad (3)$$

where I_1 and I_2 are two current rms values of the two interferers at ω_1 and $2\omega_1 - \omega_{IM3}$ while $X(\omega_1, \omega_p)$ is a factor which depends only on the relative position between the first interferer and the filter pole.¹ Equation (3) displays the same zero at $\omega_p/(g_m R_S)$ as in the noise transfer function (1), showing that noise and linearity are improved according to the same mechanism. The amount of in-band intermodulation given by (3) and that obtained using simulations are plotted in Fig. 3(a), as a function of ω_{IM3} (normalized to ω_p), in the range between 0 and ω_p . As can be seen, a good agreement is obtained over the entire frequency range considered.

In addition to the “pipe” effect, the presence of the capacitor at the input of the stage is key to ensure a high linearity in the presence of far out-of band blockers since it filters out the input interferers before entering the nonlinear device. In particular, this effect is related to the capability of the interferers to modulate the gate-source voltage of the input transistor (i.e., the nonlinear device). The magnitude of this effect can be estimated calculating the IM3 at a fixed in-band frequency ω_{IM3} as a function of the first blockers position ω_1 . Choosing for simplicity $\omega_{IM3} = 0$ Hz (i.e., IM3 product falling at DC) it follows that

$$|I_{IM3}(\omega_1)|^2 \approx |X(\omega_1, \omega_p)|^2 I_1^2 I_2. \quad (4)$$

The amount of IM3 obtained using (4) is plotted in Fig. 3(b) versus ω_1 (also in this case normalized to ω_p). For $\omega_1 \gg \omega_p$, (4) can be approximated by the following expression:

$$|I_{IM3}(\omega_1)|^2 \approx \left| \frac{3\omega_p^3 (jg_m g_3 \omega_1 + g_2^2 \omega_p)}{8g_m^5 R_S \omega_1^4} \right|^2 I_1^2 I_2 \quad (5)$$

where the IM3 product decreases as ω_1^3 .

¹For $g_m R_S \gg 1$, $\omega_p < \omega_1$, and the factor X equal to $X(\omega_1, \omega_p) = (3\omega_p^3/4g_m^4) \cdot ((g_m g_3 (2\omega_1 - j\omega_p) - 2g_2^2 \omega_p (\omega_1 - j\omega_p)) / ((\omega_1 + j\omega_p)(\omega_1 - j\omega_p)^2 (4\omega_1^2 + \omega_p^2)))$.

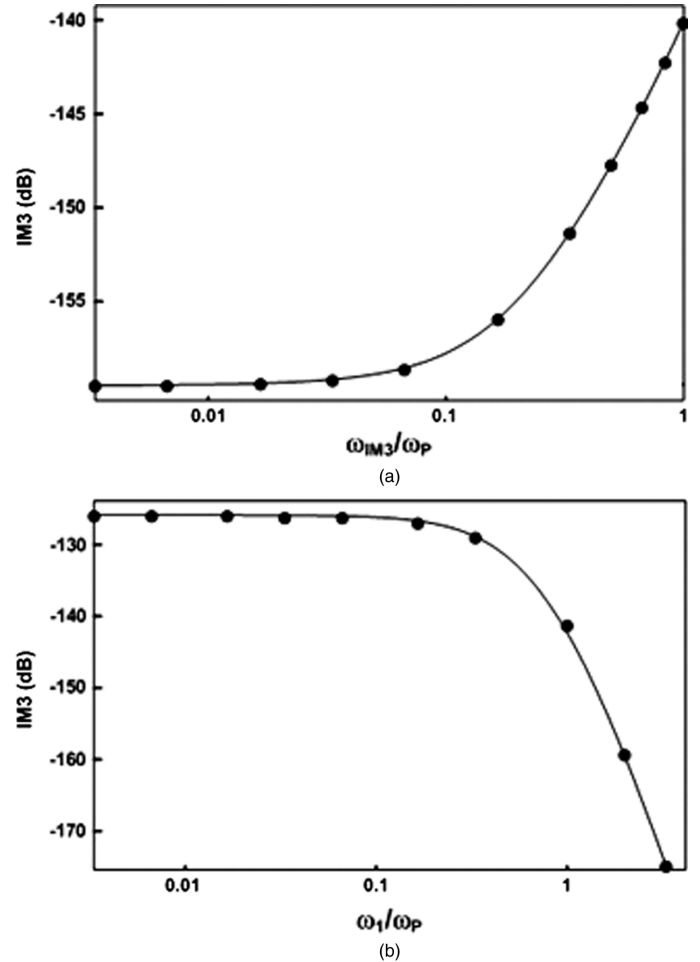


Fig. 3. First-order filter IM3 (a) versus f_{IM3} , (b) versus f_1 ($\omega_p = 2\pi * 3$ MHz, $g_m = 3.3$ mS, $g_2 = 4.4$ mA/V², $g_3 = 100$ μ A/V³, $R_S = 20$ k Ω and $I_1 = I_2 = 135$ μ A). Formulas (line) and simulation (dots).

The above behavior confirms the intuition, i.e., thanks to the filtering action provided by the input capacitance, the IM3 decreases rapidly when the two interferers are moved further away from the cut-off frequency ω_p . When the interferers fall in the passband the gate-source voltage swing is constant and with it the IM3. This is consistent with the fact that in this region the impedance at the input of the filter does not vary with frequency.

The presence of a passive blocker attenuation in front of the filter is not common to other filter topologies. For example, in standard op-amp RC structures, the current signal injected in the virtual ground is not filtered (as opposed to the voltage output). This forces the operational amplifier to sink or source the same amount of current independently of the position in frequency of the interferer signal with respect to the filter band edge.

III. BIQUAD PIPE FILTER CELL

High-order filters need both real and conjugate poles. The latter cannot be created by simply cascading two of the structure reported in Fig. 1. For a given input current signal, a pair of complex poles can be realized through the RLC network shown in Fig. 4(a). In this case the current flowing out from the inductor has a second order low-pass characteristic with a cut-off frequency ω_0 equal to the L-C resonance frequency and a quality

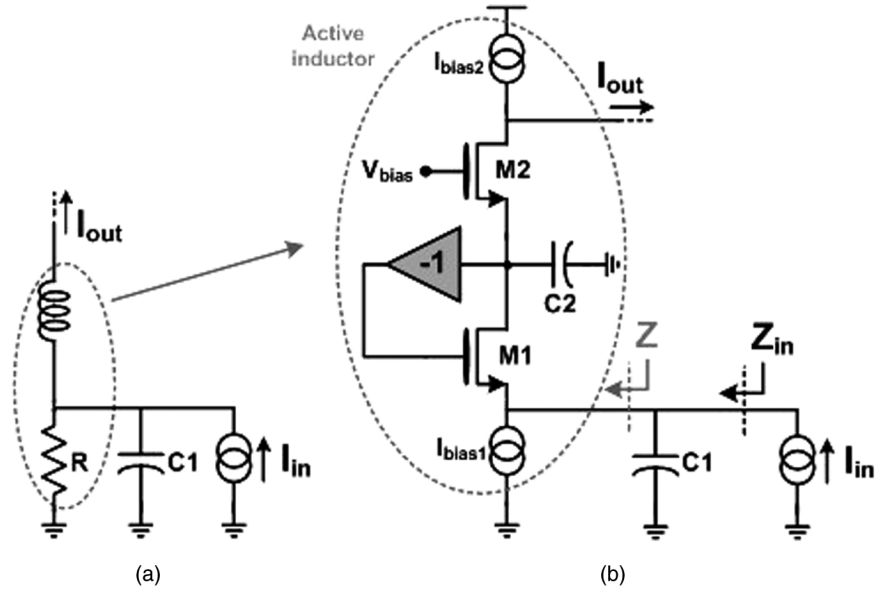


Fig. 4. Current biquad cell.

factor Q set by the shunt resistance R . Integrated inductors are generally avoided in baseband filters due to the unfeasible value of the inductances required at such frequencies. For this reason, active circuits with an inductive frequency behavior are used (e.g., the gyrator [8]).

A. Active Inductor

In the proposed biquad cell reported in Fig. 4(b), the active inductor is realized through the network formed by transistors M1–M2 and capacitor C2. At DC, the feedback closed around M1 forces the input small signal voltage at the source of M1 to be equal to the difference between the gate-source small signal voltages of M1 and M2, producing (with the use of two identical transistors) a virtual short between the input and the gate of M2. Moving from DC toward higher frequency, the presence of capacitance C2 reduces the amount of feedback around M1 and the input impedance rises as in an inductor. Computing the impedance value of Z versus frequency under the assumption of $g_{m1} = g_{m2} = g_m$, the following result is obtained:

$$Z = \frac{sC2}{g_m^2} \cdot \frac{1}{1 + sC2/g_m}. \quad (6)$$

This behavior corresponds to that of an inductance $L = C_2/g_m^2$ placed in shunt with a resistance $R = 1/g_m$. The circuit has literally “gyrated” the impedance $1/sC2$ obtaining at its input an inductance of value C_2/g_m^2 . It can be proved that, in the same way, an inductance connected at the source of M2 would be transformed into a capacitance at the input node.

B. Complex Poles

Thanks to its ability to implement an active inductor, the structure of Fig. 4(b) realizes a second-order low-pass filter with the following transfer function:

$$\frac{i_{out}}{i_{in}} = \frac{g_m^2/(C1 C2)}{s^2 + s(g_m/C1) + g_m^2/(C1 C2)} \quad (7)$$

where g_m is the transconductance of M1 and M2. The cell has an in-band current gain equal to 1, therefore it is acting as a lossless pipe where no additional current is injected into the signal path. The frequency of the conjugates poles ω_0 and their quality factor Q are given by

$$\begin{cases} \omega_0 = \frac{g_m}{\sqrt{C1 C2}} \\ Q = \sqrt{\frac{C1}{C2}} \end{cases} \quad (8)$$

Having chosen the same g_m for the two transistors, the biquad cut-off frequency ω_0 depends only on g_m and on the product of the capacitances, while the quality factor Q depends only on the $C1/C2$ ratio. While the filter transfer function has a low-pass shape, the input impedance of the filter corresponds to that of an LCR shunt resonator and is given by

$$Z_{in} = \frac{s/C1}{s^2 + s(g_m/C1) + g_m^2/(C1 C2)} \quad (9)$$

The bandpass shape of the input impedance gives a very low impedance (ideally zero) close to DC (due to the presence of the active inductor) and at extremely high frequencies (due to the capacitance C1). The maximum of the input impedance is located at ω_0 and corresponds to $1/g_m$ (i.e., the shunt loss resistance of the active inductor).

IV. BIQUAD SPURIOUS-FREE DYNAMIC RANGE

The SFDR of the solution proposed in Fig. 4(b) was computed valuating the total noise produced by the cell and the amount of distortion generated in the filter passband by a couple of interferers located far away from the channel bandwidth. The sources of noise considered were those associated with transistors M1 and M2 and the bias current generator I_{bias1} and I_{bias2} while the distortion was evaluated assuming that the only nonlinear elements are transistors M1 and M2.

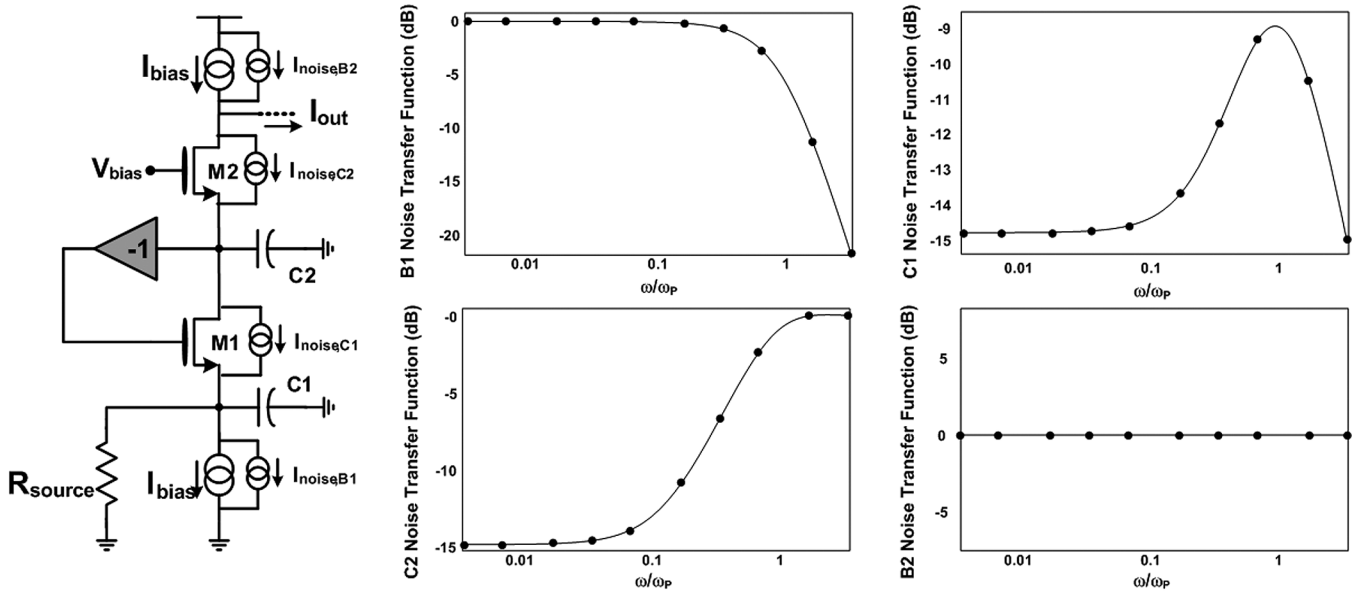


Fig. 5. Biquad cell noise transfer functions.

A. Noise

Under the assumption of white noise sources and a finite driving resistance $R_S > 1/g_m$, the transfer functions from the noise sources associated to transistors M1 and M2 to the output are given by

$$\left| \frac{i_{out}}{i_{M1}}(\omega) \right|^2 \cong \left| \frac{j\omega/\omega_p + 1/(g_m R_S)}{\omega^2/\omega_0^2 + j\omega/(\omega_0 Q) + 1} \right|^2 \quad (10)$$

$$\left| \frac{i_{out}}{i_{M2}}(\omega) \right|^2 = \left| \frac{1 - Q^2}{Q} \cdot \frac{j\omega}{\omega_0} \cdot \left(1 + \frac{j\omega}{\omega_0} \cdot \frac{Q}{1 - Q^2} \right) \right|^2 \quad (11)$$

where ω_0 and Q are given by (8) and $\omega_p = g_m/C1$. Both noise transfer functions displays a zero in the filter passband: the position of these two zero is different for the two transfer functions being a function of R_S for M1 and located in dc for M2.

Fig. 5 shows all noise transfer functions for the biquad cell, providing a comparison between theory and simulations. The main difference between the biquad and the first-order filter in the transfer function for the noise of M1 is the presence in (10) of two complex poles and one zero that produces a passband characteristic instead of a high-pass one. This is explained by the fact that the second capacitor C2 filters not only the signal but also the noise injected by M1. On the other hand, a pure high-pass transfer function is present for the noise of M2, since at frequency higher than the poles, capacitor C2 becomes a short and all the noise injected by M2 can flow to the output.

The noise associated with I_{bias1} is injected at the input and thus is processed as the input signal (i.e., without experiencing any attenuation in the filter passband) while the transfer function of I_{bias2} is flat in frequency since this noise is injected at the output of the cell. In general, these latter contributions are proportional to the transconductance of the transistors used to synthesize the current generators.

The shape of the whole output noise spectrum is qualitatively shown in Fig. 6. At low frequencies the main contributors are

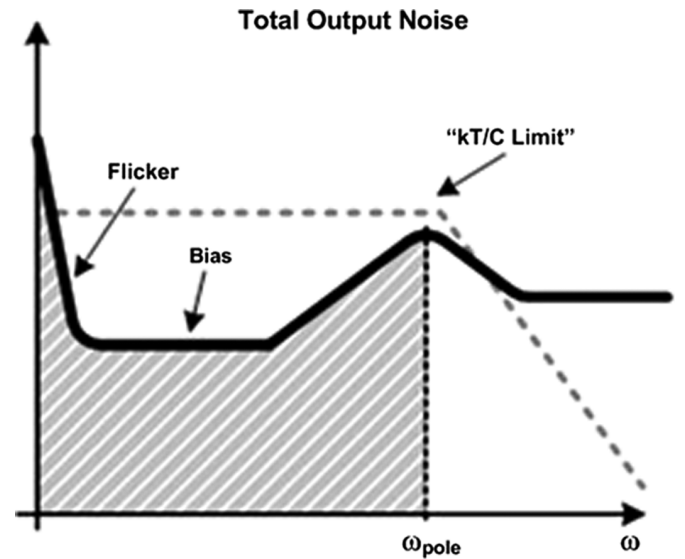


Fig. 6. Output noise summary.

the bias generators where noise is not directly related to the filter poles. On the contrary, moving toward the filter cut-off frequency, the noise contributed by M1 and M2 increases reaching its maximum at ω_0 where their noise spectral density is close to the one of classical filter topologies. Beyond the filter cut-off frequency, the only noise components that are not filtered out are those due to M2 and to the upper bias current generator. This out-of-band noise, as it will be explained in Section V, must be carefully considered because it can be folded in band when the signal is sampled at the end of the analog receiver chain, typically by an ADC.

B. Intermodulation Phenomena

As seen in Section II, the pipe filters allow to obtain high linearity taking advantage of two different mechanisms. The first is

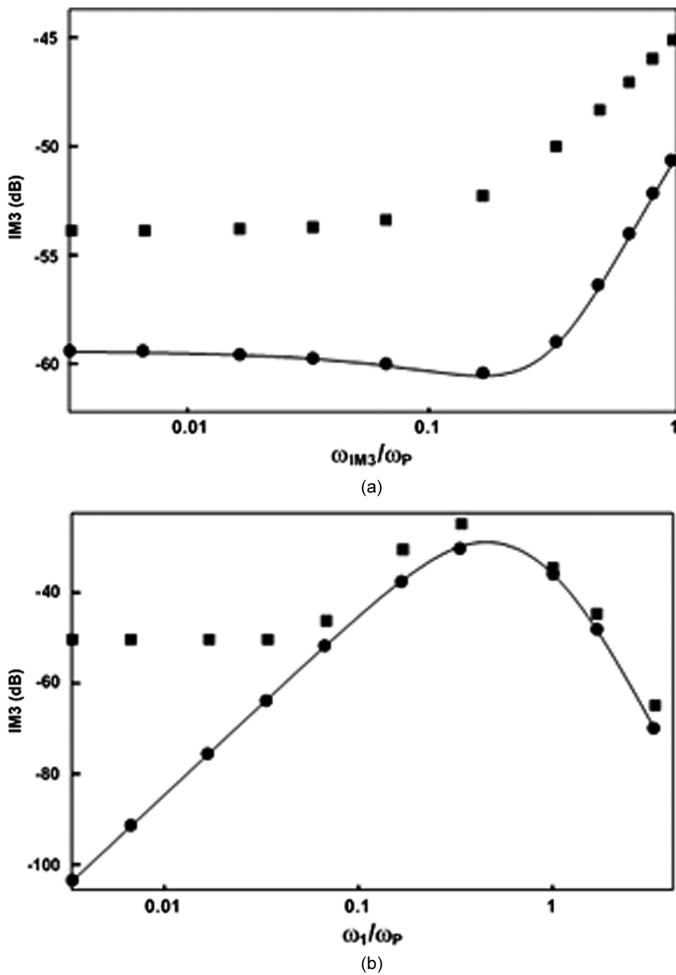


Fig. 7. Biquad cell stage IM3 (a) versus f_{IM3} , (b) versus f_1 ($\omega_p = 2\pi \cdot 3$ MHz, $Q = 0.54$, $g_m = 3.3$ mS, $g_{m,2} = 14.4$ mA/V², $g_{m,3} = -79$ μ A/V³, $R_S = 1.66$ k Ω and $I_1 = I_2 = 135$ μ A). Formulas (line) and simulation with and without finite transistor output resistance (square and dots, respectively).

the same mechanism that produces the in-band high-pass noise shaping while the second is the filtering action provided by the input capacitance. As it was done for the first-order filter, these two effects were studied also for the biquad cell, evaluating the IM3 generated by two out-of band blockers I_1 and I_2 for two different scenarios. In the first, the frequency of the intermodulation product ω_{IM3} is made to vary within the passband by placing I_1 at ω_1 and I_2 at $2\omega_1 - \omega_{IM3}$. In the second, intermodulation product ω_{IM3} is made to always fall at DC placing I_1 at ω_1 and I_2 at $2\omega_1$, while ω_1 is made to vary. Contrary to the first-order filter, where the transistor output resistance is in shunt with the transconductance and thus its impact on linearity is negligible, in this case the finite output resistance (not considered in the Volterra's analysis) affects the linearity of the cell by modifying the behavior of the feedback loop used to realize the active inductor. For this reason in Fig. 7, simulations with output resistance were also reported. Analyzing the case in which the IM3 product is made to vary across the band [Fig. 7(a)], it can be seen that in the frequency range for which the virtual ground provides a very low impedance almost all the input current flows towards the output and low distortion is produced. This behavior is equivalent to the one of the first-order filter reported in Fig. 3(a).

In Fig. 7(b), the IM3 is plotted as a function of the first blocker position ω_1 showing a passband behavior. As in the first-order topology (Section II), the IM3 frequency behavior follows the input impedance profile given by (9): rising up with frequency in the filter passband (inductive behavior), and decreasing with frequency out-of-band (capacitive behavior). The worst distortion occurs at the corner frequency, where the input impedance and the modulation across the input transistor reach their maxima.

C. Hard Distortions

To fully characterize the linearity of the biquad cell, also hard distortions have to be analyzed. These nonlinearities can influence the 1 dB compression point of the cell and occur when the signal current becomes comparable with the bias level. Thus, the higher is the bias current, the higher is the capability to handle large signal without a significant compression. Also in this case the filtering action of input capacitance C1, plays an important role and gives this filter an advantage with respect to other classical architectures. In fact, the current due to the largest input signals, typically located outside the channel bandwidth, is primarily absorbed by C1. This reduces the current entering in the filter with a consequent enhancement of the 1 dB compression point.

In conclusion, the current mode biquad cell proposed has two important properties making it very suitable for use in a receiver chain. First, it achieves low noise in the signal band, where a high signal-to-noise ratio is the key target. Second, its linearity increases as the input signal is moved far away from the band edge. This latter behavior fits the linearity requirement of a typical wireless receiver where most of the input signal power is located out-of-band (interferers) [9]. Furthermore the interferer power tends to increase proportionally to its distance from the filter band edge (channel bandwidth).

V. DESIGN OF 4TH WCDMA CHANNEL SELECTION BASEBAND FILTER

To validate the theory reported above, a 4th-order Butterworth filter intended to perform channel selection in a WCDMA receiver was designed and integrated in 65 nm CMOS technology. The filter was implemented as the cascade of two current biquad cells like the one of Fig. 4 (adopting a fully-differential architecture to easily implement the sign inversion in the feedback network). A complete scheme of the structure is drawn in Fig. 8. The filter was designed to operate after a current mixer that, for its nature, behaves as a current signal source. In this case, however, for testing purpose, two resistances (R1) were connected to the input to implement a V-I converter. This was possible since this structure has a very low in-band input impedance. Also for ease of testing, the output current was converted to voltage on the differential resistor R2. The relative noise contribution of R2 decreases as R2 is increased. In fact, while the noise added by R2 is proportional to its value, all the other contributes are amplified by the square of R2. The maximum feasible value for R2 is limited by the maximum swing at the cell output. However, most of the input energy is located out of band and it is filtered out before reaching R2. As a consequence R2 can be chosen sufficiently high (20 k Ω) to make its noise contribution negligible (less than 2% of the total).

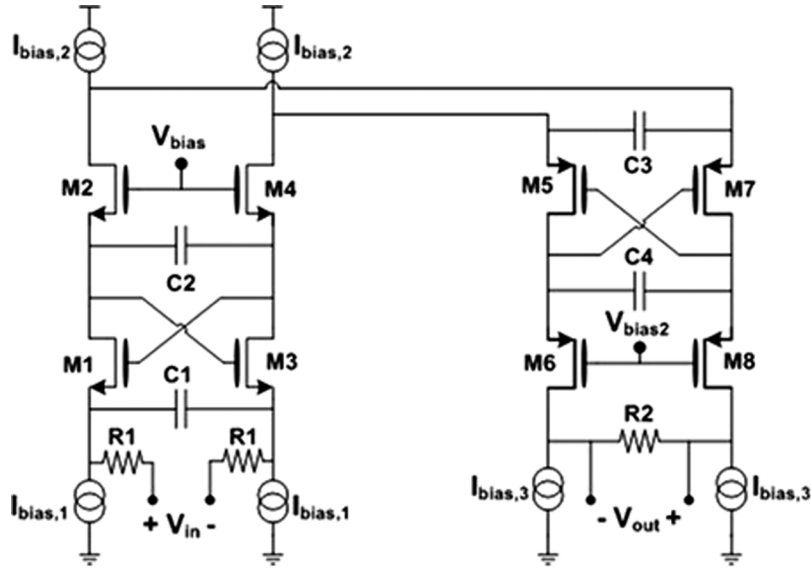


Fig. 8. Fourth-order filter schematic.

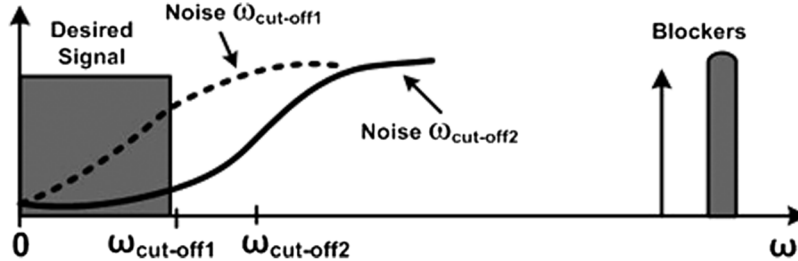


Fig. 9. Choice of cut-off frequency.

A. Design Strategies for Pipe Filter Cascade

One of the first steps in a filter design is the choice of the cut-off frequency ($\omega_{\text{cut-off}}$). In classic filters, where noise and signal have roughly the same transfer function, this frequency is generally minimized to maximize the blockers attenuation. Indeed, a higher $\omega_{\text{cut-off}}$ would not produce any benefit on the in-band SNR, since both the noise and the signal are processed by the same transfer function [10]. For a pipe filter however, the presence of in-band noise shaping makes this choice less obvious, as it is qualitatively shown in Fig. 9. If $\omega_{\text{cut-off}}$ is moved beyond the channel bandwidth, due to the difference in the noise and signal transfer functions a significant improvement of SNR is produced. However, this benefit trades off with the requirements of selectivity that depends on the position and on the amplitude of the input interferers. In the case of a WCDMA receiver, the scenario considered by the standard assumes the presence of two interferers at 10 MHz and 20 MHz, with well defined energies [9]. On the base of these requirements a compromise $\omega_{\text{cut-off}} = 2.8$ MHz, that is 1.45 times the channel bandwidth (i.e., 1.92 MHz), was chosen.

The second step in the filter design is the definition of the bias current for each stage. This value must be greater or equal to the largest between the minimum current necessary to handle the interferers and the minimum current that allows to satisfy the condition $g_m \gg 1/R_S$ required for a proper operation of the filter (see Section II). Although in general the first condition is the

more stringent, the use of a mixer as driving stage could require a higher bias current to keep negligible the effect of the finite impedance of the down-converter on the filter transfer function [11]. In this design, since the input capacitance $C1$ attenuates the blocker at 10 MHz by almost 10 dB and the one at 20 MHz by almost 16 dB (being $\omega_{\text{cut-off}} = 2.8$ MHz), the bias current can be three times smaller than the one that would be required to manage the full interferer. For the same reason, the bias current of the second stage can be reduced by another factor of ten since the 10 MHz blocker is attenuated by an additional 20 dB by the first stage. The minimum bias current required by the second stage is lower also because the first stage provides an output impedance larger than R_S (i.e., $R_S \cdot (g_m/g_{ds})$).

The final step is to choose the transconductances and the capacitances of the cell that minimize the noise and maximize the signal voltage swing compatibly with the supply voltage. The impedance levels can be increased moving down the filtering chain because each stage increases the driving impedance for the following stage and contributes in the filtering of out-of-band interferers. The impedance scaling gives also a reduction of the silicon area since smaller capacitances are needed. For the solution proposed, the transconductances of the two stages have been set respectively to 3.3 mS for the first cell and 330 μ S for the second one.

In Table I the design parameters for all transistors are reported. Notice that the overdrive of the current generators is

TABLE I
FILTER PROTOTYPE TRANSISTORS PARAMETERS

	I _{bias} Current [μ A]	W/L [μ m/ μ m]	Overdrive Voltage [mV]	g_m [mS]
I _{bias.1}	240	24/10	764	0.565
M1/M2/M3/M4	240	144/2	110	3.35
I _{bias.2}	264	132/10	715	0.664
M5/M6/M7/M8	24	12/0.5	131	0.34
I _{bias.3}	24	24/10	219	0.2

much larger than that of M1–M2 to minimize their contribution to the in-band noise.

B. Out-Band Noise Folding

The out-of-band noise present at the output of a pipe filter can be folded down during the sampling phase that occurs within the ADC. For this reason this noise has to be minimized to maintain an advantage compared to traditional solutions, where most of the noise lies in the filter passband.

The out-of-band noise in a pipe filter is contributed only by the last stages of the filtering chain that have a high-pass transfer function (e.g., the noise of M2 and of I_{bias2} in Fig. 5). This noise is proportional to the bias current that, as shown in the previous section, is scaled down in the last stage. Finally, since in general the current signal has to be converted to voltage before entering the ADC, an additional pole can be added at the end of the pipe filter, placing a capacitor in parallel with the load resistance, providing a further attenuation of the out-of-band noise. Introducing this additional pole does not require a large capacitance since a large resistor can be used at the output where most of the interferers are already filtered.

Due to the above, in the proposed design the out-of-band noise (obtained integrating it from the filter corner $\omega_{cut-off}$ to “infinite”) is less than one third of the in-band noise. This means that, even sampling the output at the Nyquist rate, which is rarely done, the in-band noise after sampling would increase less than 1 dB.

VI. EXPERIMENTAL RESULTS

The chip micrograph of the filter prototype, fabricated in a 90 nm CMOS process, is shown in Fig. 10. All pads are ESD protected and the active die area is 0.5 mm². This area is dominated by low-density MiM capacitors (210 pF), whose placement could be further improved, resulting in a lower area occupation. Moreover, large on-chip MoM bypass capacitors are used to filter the noise on the supply voltage with respect to ground. The die was bonded on a dedicated double-side RF board, realized on an FR4 substrate. Gold strip lines, optimized to reduce their area occupation, carry the signals from the input connectors to the die. As discussed in the previous section, the voltage-to-current conversion is performed placing two resistances (R1) of 1.66 k Ω in series with the input while the output signal is sensed on a resistor (R2) of 20 k Ω . The plot of the filter frequency response versus frequency from DC to 20 MHz is shown in Fig. 11 together with the response of the ideal 4th-

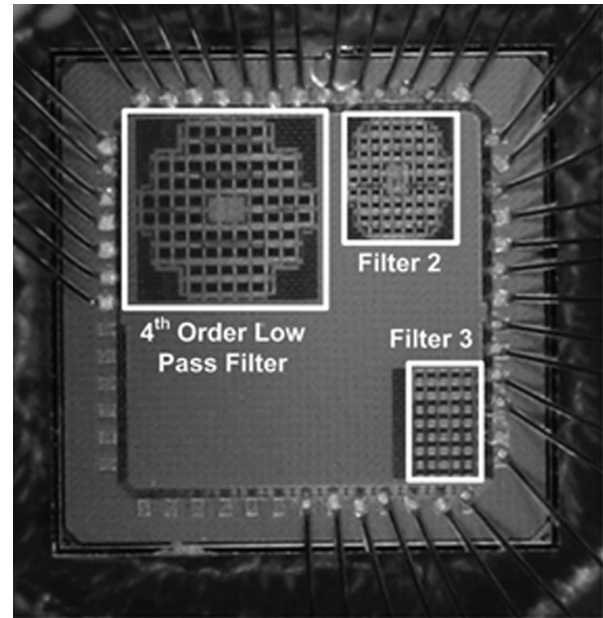


Fig. 10. Chip micrograph.

order Butterworth filter used for the design. The plot is obtained de-embedding the effect of the parasitic pole caused by the capacitive load associated with the probe (about 5 pF). The DC gain is about 15 dB, due to the ratio between the output and the input resistors, and the filter cut-off frequency is close to 2.8 MHz as expected from the simulations. When the out-of-band attenuation reaches about 55 dB the plot levels off due to a parasitic leakage on the board. This was proved by measuring the input to output transfer function with the filter powered off.

The output noise spectrum was measured shorting the differential inputs of the die in front of the R1 resistance. In this way the effect of the finite driving impedance (i.e., the output resistance of the mixer in a receiver chain) on the filter output noise is included. At the receiver output an active probe with a 20 dB gain was used to raise the filter noise above the sensitivity level of the spectrum analyzer. The measured output noise spectrum is reported in Fig. 12 compared with the simulated one. The noise transfer function has a bandpass shape as expected from the theory. The noise spectrum shows a minimum equal to -128.5 dBm/Hz, located in the filter band, where the main contributors are the bias generators. Below that $1/f$ noise dominates while near the corner frequency, where the main contributors are the filtering transistors, there is a local maximum equal to -123 dBm/Hz. At higher frequencies the output noise decreases because all contributors are filtered out by the filter itself and by the parasitic output pole. The $1/f$ corner is located at 25 kHz. This output noise frequency behavior is consistent with the theory, as shown by the solid line in Fig. 12. The out-of-band IIP3 is 35.6 dBm, and it has been measured with two tones, the first placed at 10 MHz and the second at 19.5 MHz, that give a third-order intermodulation product at 500 kHz. Fig. 13 shows the simulated (dots) and measured (squares) filter IIP3, versus the frequency of the IM3 product [Fig. 13(a)] and versus the frequency of the first blocker f_1 [Fig. 13(b)]. These frequencies are kept the same, with respect to the plots in Section IV. The

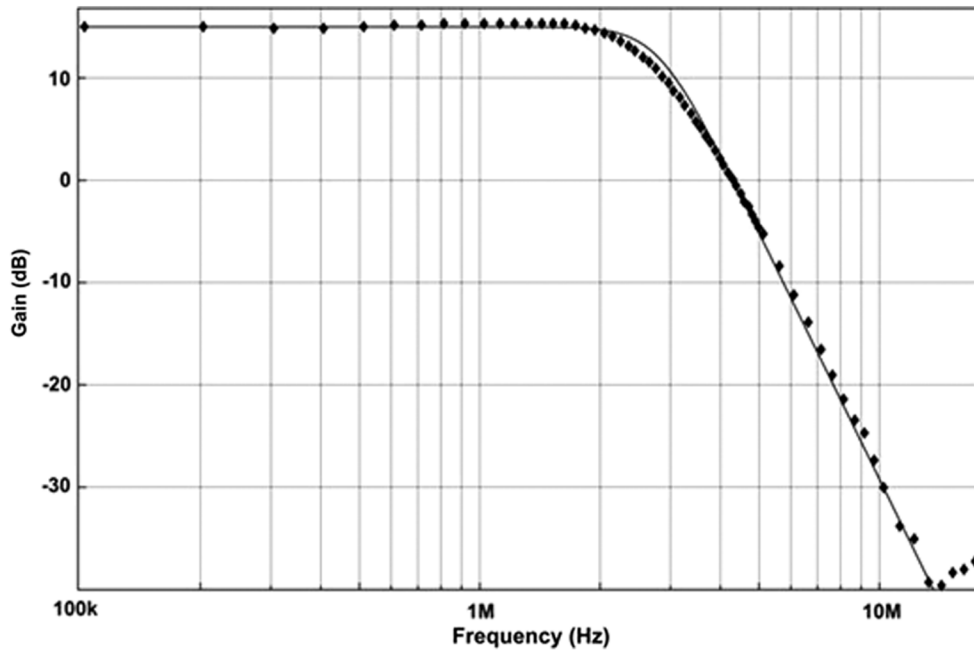


Fig. 11. Measured output transfer function.

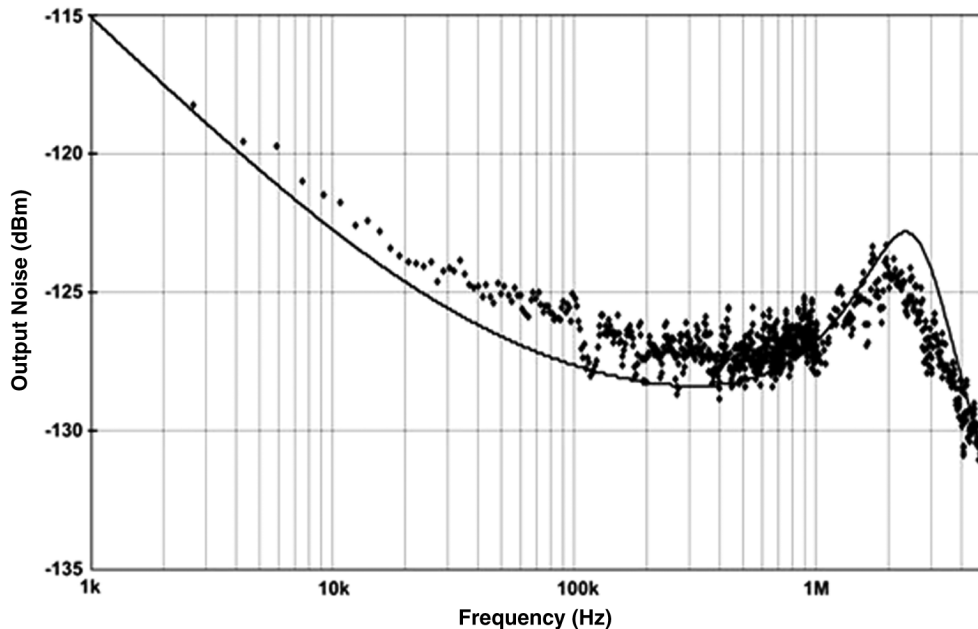


Fig. 12. Measured output noise function.

measurements fit very well with the simulations, confirming the theory.

A summary of the most relevant measurements and a comparison with the state of art for filters designed for the same applications (WCDMA) is reported in Table II. In particular this work has the lowest power consumption, equal to 1.26 mW, with an SFDR higher than all but one of the other filters. The filter cut-off frequency is set to 2.8 MHz, i.e., about 40% larger than the UMTS bandwidth that is equal to 1.92 MHz. This gives a significant in-band noise improvement while still providing sufficient selectivity. Finally, the figure of merit (FoM) (based on [1]) is almost 6 dB better than the next best one. Two more versions of the filter were also fabricated, where the capacitors are

scaled down by a factor of six (Table III). One of these scaled filters (called filter 2) is operated from a 2.5 V supply while the other (called filter 3) is operated from a 1.8 supply. Filter 2 uses input resistors scaled up by a factor slightly higher than 6 and has a slightly better FoM than the un-scaled filter. For the case of filter 3, the input resistors are increased close to the maximum feasible value which still allows to reach full scale swing at the output without exceeding the supply with the input signal. In this situation a much greater linearity is obtained together with a relatively small increase in noise. This results in a further improvement of the FoM (2 dB with respect to filter 2, 6 dB with respect to the un-scaled filter and 12 dB with respect to the state of the art).

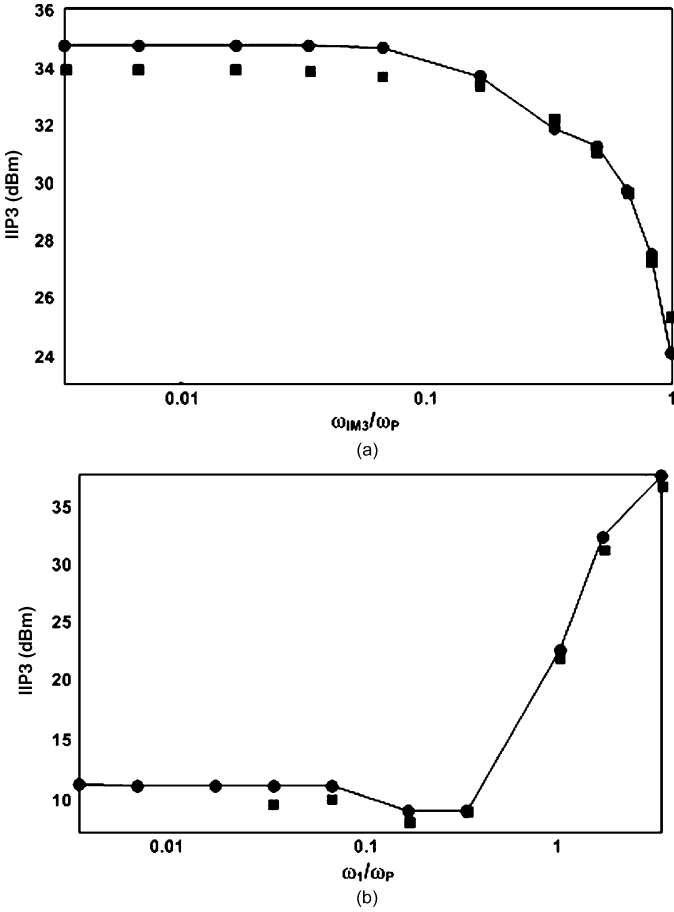


Fig. 13 Fourth-order filter IIP3 (a) versus f_{IM3} , (b) versus f_1 . Simulation (dots) and measurements (squares).

TABLE II
FILTER PROTOTYPE MEASUREMENTS AND COMPARISON
WITH THE STATE OF THE ART

	This Work	[10]	[1]	[12]	[13]	[14]
Voltage Supply [V]	2.5	1.2	2.7	1.8	2.5	1.2
DC Power [mW]	1.26	3.4	6.21	4.86	7.3	1.8
Cut-freq [MHz]	2.8	2.11	1.92	2	2.2	2.75
Number of Poles	4	4	5	5	3	5
IIP3 Out of Band [dBm]	35.6	31	41	33	15	24
Input referred noise [μV_{RMS}]	32	36	47	80	52	116
SFDR Out of band [dB]	75	71.25	76.5	68	58.5	59.75
FoM [dB]	-174	-165	-168	-161	-148	-159

VII. CONCLUSION

A class of filters based on the concept of pipe filtering was presented. In the filter passband, such kinds of structures behave like lossless pipes where no noise or distortion can be added to the signal. This results in an in-band zero in both noise

TABLE III
2.5 V (FILTER 2) AND 1.8 V (FILTER 3) SCALED VERSIONS

	Filter 2	Filter 3
Voltage Supply [V]	2.5	1.8
DC Power [mW]	0.21	0.15
Cut-freq [MHz]	2.8	2.8
Number of poles	4	4
Gain [dB]	-1	-7
IIP3 Out of Band [dBm]	40.7	48.5
Input referred noise [μV_{RMS}]	126	273
SFDR Out of band [dB]	70.43	71.18
FoM [dB]	-178	-180

and IM3 transfer functions. Furthermore, passive filtering action provided by the capacitance at the input of the filter improves linearity. Thanks to these properties, such filters consume less area and power than the conventional ones, especially when operating with strong interferers moderately far from the channel band (as is the case of wireless receiver chains).

APPENDIX I

CURRENT VERSUS VOLTAGE OUTPUT

In the current-driven gm-C filter reported in Fig. 1, there are two different ways to take the output: the first is to sense the signal as a voltage across the capacitor (V_{out}), and the second is to detect the current flowing out of the transistor (I_{out}). Although in both cases the input-output transfer function is a first-order low-pass filter (with a single real pole located at $\omega_p = g_m/C$), the output noise is different. In the case of a voltage output, the noise introduced by the transistor is filtered according to the signal transfer function, while in the current-mode approach (with $R_S = \infty$), the noise transfer function has a zero at DC, leading to high-pass shaping [Fig. 1(b)]. The difference between the two approaches is a significant in-band noise reduction in favor of the current-mode one. In particular, the output noise integrated from DC to the filter cut-off frequency ω_P for the two cases is

$$v_{noise}^2 = kT/(2C) = kT\omega_P/(2g_m) \quad (12)$$

$$i_{noise}^2 = 0.14kT\omega_P^2C = 0.14kT\omega_Pg_m \quad (13)$$

where k is the Boltzmann's constant, T is the temperature, v_{noise}^2 is the voltage noise power across the capacitance, and i_{noise}^2 is the current noise power flowing out of the transistor.

In terms of SNR, a comparison can be done assuming the same in-band input signal, i.e., an input current power equal to i_{in}^2 . This corresponds to an output voltage power $v_{out}^2 = i_{in}^2/g_m^2$ and an output current power $i_{out}^2 = i_{in}^2$. From (12) and (13), the SNR for the two configurations becomes

$$SNR_{voltage} = \frac{v_{out}^2}{v_{noise}^2} = \frac{i_{in}^2}{0.5kTg_m\omega_P} \quad (14)$$

$$\text{SNR}_{\text{current}} = \frac{i_{\text{out}}^2}{i_{\text{noise}}^2} = \frac{i_{\text{in}}^2}{0.14 \cdot kTg_m\omega_P}. \quad (15)$$

This corresponds to 5.6 dB better SNR in favor of the current-mode one.

ACKNOWLEDGMENT

The authors thank Marvell for technology access, and Steve Shia of TSMC for his support.

REFERENCES

- [1] A. Yoshizawa and Y. P. Tsividis, "Antiblocker design techniques for MOSFET-C filters for direct-conversion receivers," *IEEE J. Solid-State Circuits*, vol. 37, no. 3, pp. 357–364, Mar. 2002.
- [2] Castello and Gray, "Performance limitations in switched-capacitor filters," *IEEE Trans. Circuits Syst.*, vol. 32, no. CAS-9, pp. 865–876, 1985.
- [3] A. Liscidini, A. Pirola, and R. Castello, "A 1.25mW 75dB-SFDR CT filter with in-band noise reduction," in *IEEE Int. Solid-State Circuits Conf. (ISSCC) Dig. Tech. Papers*, 2009, pp. 336–337.
- [4] A. Tekin, H. Elwan, K. Pedrotti, and N. Dogan, "Noise-shaped post-mixer blocker filter for integrated receivers," in *Int. Conf. Microelectronics*, Dubai, Dec. 2008.
- [5] A. Tekin, H. Elwan, A. Ismail, and K. Pedrotti, "Noise-shaping gain-filtering techniques for integrated receivers," *IEEE J. Solid-State Circuits*, vol. 44, no. 10, pp. 2689–2693, Oct. 2009.
- [6] D. D. Weiner and J. F. Spina, *Sinusoidal Analysis and Modeling of Weakly Nonlinear Circuits*. New York: Van Nostrand Reinhold, 1980.
- [7] P. Wambacq and W. Sansen, *Distortion Analysis of Analog Integrated Circuits*. Boston, MA: Kluwer, 1998.
- [8] A. Antoniou, "Gyrator using operational amplifier," *Electron. Lett.*, vol. 3, pp. 350–352, 1967.
- [9] O. K. Jensen, T. E. Kolding, C. R. Iversen, S. Laursen, R. V. Reynisson, J. H. Mikkelsen, E. Pedersen, M. B. Jenner, and T. Larsen, "RF receiver requirements for 3G WCDMA mobile equipment," *Microwave J.*, vol. 43, no. 2, pp. 22–46, 2000.
- [10] S. D'Amico, V. Giannini, and A. Baschiroto, "A 4th-order active Gm-RC reconfigurable (UMTS/WLAN) filter," *IEEE J. Solid-State Circuits*, vol. 41, no. 7, pp. 1630–1637, Jul. 2006.
- [11] M. Valla, G. Montagna, R. Castello, R. Tonietto, and I. Bietti, "A 72-mW CMOS 802.11a direct conversion front-end with 3.5-dB NF and 200-kHz 1/f noise corner," *IEEE J. Solid-State Circuits*, vol. 40, no. 4, pp. 970–977, Apr. 2005.
- [12] A. Yoshizawa and Y. P. Tsividis, "A channel-select filter with agile blocker detection and adaptive power dissipation," *IEEE J. Solid-State Circuits*, vol. 42, no. 5, pp. 1090–1099, May 2007.
- [13] D. Chamla, A. Kaiser, A. Cathelin, and D. Belot, "A Gm-C low-pass filter for zero-IF mobile applications with a very wide tuning range," *IEEE J. Solid-State Circuits*, vol. 40, no. 7, pp. 1143–1450, Jul. 2005.
- [14] D. Chamla, A. Kaiser, A. Cathelin, and D. Belot, "A switchable-order Gm-C baseband filter with wide digital tuning for configurable radio receivers," *IEEE J. Solid-State Circuits*, vol. 42, no. 7, pp. 1513–1521, Jul. 2007.



Alberto Pirola (S'07) received the M.Sc. degree (*summa cum laude*) in microelectronic engineering from the University of Pavia, Italy, in 2007. Currently he is working towards the Ph.D. degree at the University of Pavia in the Microelectronics Laboratory.

His research interests are in the implementations of analog RF front-end in CMOS technology, with particular focus on high SFDR current-driven baseband filters.



Antonio Liscidini (S'99–M'06) received the Laurea degree (*summa cum laude*) and the Ph.D. in electrical engineering from the University of Pavia, Pavia, Italy, in 2002 and 2006, respectively.

He was a summer intern at National Semiconductors, Santa Clara, CA, in 2003 studying poly-phase filters and CMOS LNA. Currently he is an Assistant Professor at the University of Pavia. His research interests are in the implementations of analog RF front-end in CMOS and BiCMOS technology, with particular focus on the analysis and design of LNAs

for multi-standard applications, ultralow-power receivers and digital PLLs. In addition to his academic activities, he has been acting as a consultant for Marvell Semiconductors in the area of integrated circuit design.

Dr. Liscidini received the Best Student Paper Award at IEEE 2005 Symposium on VLSI Circuits. Since December 2007, he has served as an Associate Editor of the IEEE TRANSACTIONS ON CIRCUITS AND SYSTEMS II: EXPRESS BRIEFS and since 2010 he has been a member of the TPC of the European Solid State Circuit Conference (ESSCIRC).



Rinaldo Castello (S'78–M'78–SM'92–F'99) graduated from the University of Genova (*summa cum laude*) in 1977 and received the M.S. and the Ph. D. degrees from the University of California, Berkeley, in 1981 and 1984.

From 1983 to 1985 he was Visiting Assistant Professor at the University of California, Berkeley. In 1987 he joined the University of Pavia, Italy, where he is now a Full Professor. He consulted for ST-Microelectronics, Milan, Italy, up to 2005 and from 1998 to 2005 was the Scientific Director of a joint research centre between the University of Pavia and ST. He promoted the establishment of several design centers from multinational IC companies in the Pavia area, including Marvell, for which he has been consulting since 2005.

Dr. Castello has been a member of the TPC of the European Solid State Circuit Conference (ESSCIRC) since 1987 and of the International Solid State Circuit Conference (ISSCC) from 1992 to 2004. He was Technical Chairman of ESSCIRC '91 and General Chairman of ESSCIRC'02, Associate Editor for Europe of the IEEE JOURNAL OF SOLID-STATE CIRCUITS from 1994 to 1996 and Guest Editor of the July 1992 special issue. From 2000 to 2007, he was a Distinguished Lecturer of the IEEE Solid-State Circuits Society. He was named one of the outstanding contributors for the first 50 years of the ISSCC and was a co-recipient of the Best Student Paper Award at the 2005 Symposium on VLSI.